Available online at www.sciencedirect.com
SCIENCE DIRECT®
International Journal of Heat and Mass Transfer 48 (2005) 3035–3046
International Journal of HEAT and MASS TRANSFER
www.elsevier.com/locate/ijhmt

Numerical simulation data for assessment of particle-laden turbulent flow models

K. Sengupta, K. Russell, W.J. Minkowycz, F. Mashayek *

Department of Mechanical and Industrial Engineering, University of Illinois at Chicago, 842 West Taylor Street, Chicago, IL 60607, USA

Received 3 January 2005; received in revised form 4 March 2005

Abstract

This paper presents a collection of numerical simulation data which provides a reference for the assessment of various statistical/stochastic models in incompressible homogeneous particle-laden turbulent flows. Four different homogeneous flow configurations are studied, namely, homogeneous shear flow, homogeneous plane strain flow, homogeneous axisymmetric expansion and contraction. An Eulerian–Lagrangian formulation is used for the two-phase flow simulation. A Fourier pseudospectral method is used for the solution of the Eulerian carrier-phase equations without resorting to any turbulence model. The Lagrangian equations for the dispersed phase are integrated using a modified Stokes drag. For the shear flow, both monodispersed and polydispersed particles have been considered. In this paper, only the results that are relevant for assessment of various statistical models for both the fluid and dispersed phases are presented.
© 2005 Elsevier Ltd. All rights reserved.

1. Introduction

The objective of this work is to provide a comprehensive data bank from numerical simulation of a variety of incompressible homogenous particle-laden turbulent flows, which can be used for the assessment of statistical/stochastic models. The applicability of similar data for such model validations has been demonstrated in our previous works in, for example, Reynolds average Navier–Stokes (RANS) [1], probability density function (PDF) [2], and stochastic [3] modeling. In this study, we use direct numerical simulation (DNS) for the carrier phase in an Eulerian frame whereas the particles are tracked in a Lagrangian frame. A modified Stokes drag is used to describe the coupling between the two phases.

Four different anisotropic particle-laden turbulent flows with low volume fraction and high density ratio are considered. The first is a homogeneous shear flow for which the instantaneous carrier-phase velocity is described as

$$\widehat{U}_\alpha = U_{1,2}x_2\delta_{\alpha 1} + u_\alpha, \quad \alpha = 1,2,3. \tag{1}$$

Here, $\widehat{\ }$ denotes the instantaneous quantity, u_α is the fluctuating carrier-phase velocity, δ_{ij} is the Keroneker delta function, and $U_{1,2} = \mathrm{d}U_1/\mathrm{d}x_2 =$ constant, with x_1 and x_2 indicating the streamwise and cross-stream flow directions, respectively. The mean velocity $U_\alpha = \langle \widehat{U}_\alpha \rangle$ is calculated by (Eulerian) ensemble averaging (denoted by $\langle\ \rangle$) over the number of grid points. It is noted that the homogeneous shear flow is identified by one shear component in the mean velocity gradient tensor.

* Corresponding author. Tel.: +1 312 996 1154; fax: +1 312 413 0447.
E-mail address: mashayek@uic.edu (F. Mashayek).

0017-9310/$ - see front matter © 2005 Elsevier Ltd. All rights reserved.
doi:10.1016/j.ijheatmasstransfer.2005.03.003

Nomenclature

B_{ij}	coordinate transformation tensor
d_{p}	particle diameter
f	$(1+0.15Re_{\mathrm{p}}^{0.687})$
k	turbulence kinetic energy
m_{p}	particle mass
$\widehat{P}$	instantaneous pressure
Re_0	box Reynolds number
Re_{p}	particle Reynolds number
S_{ij}	strain rate tensor
St	non-dimensional time
$\widehat{U}_i$	instantaneous velocity of the carrier phase
$\widehat{U}_i^*$	instantaneous velocity of the carrier phase at the particle position
U_i	carrier-phase mean velocity
u_i	carrier-phase fluctuating velocity
$\widehat{V}_i$	particle instantaneous velocity
v_i	particle fluctuating velocity
X_i	particle position

Greek symbols

ρ_{p}	particle density
μ	dynamic viscosity of the carrier fluid
Φ_{m}	particle mass loading ratio
ξ_i	moving coordinate
ϵ	isotropic rate of dissipation
τ_{p}	non-dimensional particle time constant

In contrast, the other flows considered in this study are formed with only normal components of the mean velocity gradient tensor without any shear component. These include three flows: plane strain, axisymmetric contraction, and axisymmetric expansion, with an instantaneous carrier-phase velocity described as

$$\widehat{U}_\alpha = U_{\alpha,\alpha}x_\alpha + u_\alpha, \quad \alpha = 1,2,3. \tag{2}$$

where $U_{\alpha,\alpha}$ = constant with no summation over Greek indices. The intensity (or rapidity) of the mean strain rate, referred to as "equivalent mean strain rate [4]", can be measured in terms of $S = (S_{ij}S_{ij}/2)^{1/2}$ where $S_{ij} = (U_{i,j} + U_{j,i})/2$ and summation over repeated indices is implied. We have for shear flow

$$S_{ij} = S\begin{pmatrix} 0 & 1 & 0 \\ 1 & 0 & 0 \\ 0 & 0 & 0 \end{pmatrix}, \tag{3}$$

for plane strain flow

$$S_{ij} = S\begin{pmatrix} 1 & 0 & 0 \\ 0 & -1 & 0 \\ 0 & 0 & 0 \end{pmatrix}, \tag{4}$$

for axisymmetric contraction flow

$$S_{ij} = \frac{2S}{\sqrt{3}}\begin{pmatrix} 1 & 0 & 0 \\ 0 & -1/2 & 0 \\ 0 & 0 & -1/2 \end{pmatrix}, \tag{5}$$

and for axisymmetric expansion flow

$$S_{ij} = \frac{2S}{\sqrt{3}}\begin{pmatrix} -1 & 0 & 0 \\ 0 & 1/2 & 0 \\ 0 & 0 & 1/2 \end{pmatrix}. \tag{6}$$

These simple homogeneous flows can approximate various regions in a more complex flow. For example, the circulation zone behind the step in a backward-facing step flow can be approximately represented by a plane strain flow, while the shear layer formed between the higher and lower halves of the channel after the step, may be approximated by a homogeneous shear flow. As a result, these flows can be used for a preliminary assessment of various turbulence models, prior to their implementations in more realistic flows with complex geometries. There are also some subtle differences among the aforementioned homogeneous flows that could be utilized for assessing various aspects of the models. For example, in the plane strain and axisymmetric flows, there is a mean velocity difference between the carrier and dispersed phases. This creates an opportunity to address several fundamental issues in two-phase turbulent flows, such as the so-called "crossing trajectories effect". Further, although the carrier phase is incompressible, the dispersed phase behaves as "compressible" and its volume changes as a function of time. Capturing the fundamental phenomena such as these could be considered as stringent tests for statistical models which are often derived following a long and tedious mathematical procedure while making many simplifying assumptions.

In the next section the formulation and numerical issues are discussed. In Section 3 the results of the simulations are presented, followed by some concluding remarks in Section 4.

2. Formulation

The carrier and dispersed phases are simulated in the Eulerian and Lagrangian frames, respectively. All the variables are normalized using reference scales for length (L_0), velocity (U_0), and density (ρ_0). The length scale is conveniently chosen such that the normalized volume of the simulation box is $(2\pi)^3$, and the fluid density is

used as the scale for density. The velocity scale is found from the box Reynolds number, $Re_0 = \rho_0 U_0 L_0/\mu$ which is specified based on the grid resolution adopted for the simulations. The governing equations are described by the instantaneous continuity and momentum equations for the fluid

$$\frac{\partial \widehat{U}_j}{\partial x_j} = 0,$$
$$\frac{\partial \widehat{U}_i}{\partial t} + \frac{\partial(\widehat{U}_i \widehat{U}_j)}{\partial x_j} = -\frac{\partial \widehat{P}}{\partial x_i} + \frac{1}{Re_0}\frac{\partial^2 \widehat{U}_i}{\partial x_j \partial x_j} - \frac{f}{\Delta V}\sum^{n_p} \frac{m_p(\widehat{U}_i^* - \widehat{V}_i)}{\tau_p}, \tag{7}$$

along with the Lagrangian equations of motion for a single particle

$$\frac{dX_i}{dt} = \widehat{V}_i, \quad \frac{d\widehat{V}_i}{dt} = \frac{f}{\tau_p}(\widehat{U}_i^* - \widehat{V}_i). \tag{8}$$

Here * denotes the carrier-phase variable evaluated at the particle position. The nondimensional particle time constant (based on the Stokesian drag for a spherical particle) is defined as $\tau_p = Re_0 \rho_p d_p^2/18$ where ρ_p and d_p are the particle density and diameter, respectively. The function $f = 1 + 0.15Re_p^{0.687}$ in (7) and (8), represents a correction to the Stokes drag relation at high particle Reynolds number ($Re_p = Re_0 d_p \mid U_i^* - V_i \mid \leqslant 1000$). The last term in (7) describes the effects of the particles on the fluid (i.e. the two-way coupling). This Eulerian source/sink term is calculated from the Lagrangian particles by summing over the number of the particles, n_p, present in the Eulerian cell of volume ΔV.

The primary objective of the simulations is to furnish statistics of the fluctuating velocities for the assessment of statistical models. This, however, requires the knowledge of the mean velocities of the particle phase—note that the mean velocity of the carrier phase is known a priori. While this information can be provided by averaging over various realizations as well as the homogeneous (x_3) direction of the flow, the number of the realizations (needed to provide accurate and meaningful statistics) is estimated to be very large [5]. Therefore, we adopt an alternate approach to provide analytical solutions for the mean velocity of the particle phase. The approach has been described in detail in our previous works [6,7]; here we provide only a brief description, mainly to highlight the limitations imposed on the flows that can be considered.

We begin by ensemble averaging the particle momentum equation (8) (which, under the present conditions, may also be viewed as an Eulerian equation for the dispersed phase [8])

$$\frac{D^V V_i}{Dt} = \ll \frac{f}{\tau_p}(\widehat{U}_i^* - \widehat{V}_i) \gg - \ll v_j \frac{\partial v_i}{\partial x_j} \gg . \tag{9}$$

Here $\frac{D^V}{Dt} = \frac{\partial}{\partial t} + V_j \frac{\partial}{\partial x_j}$, the notation $\ll \gg$ denotes the ensemble average associated with the dispersed phase, and V_i ($= \ll \widehat{V}_i \gg$) and v_i are the particle mean and fluctuating velocities, respectively. For a homogeneous dispersed phase, it can be shown [6] that the last correlation in (9) vanishes. Then, substituting from (1) for the carrier-phase mean velocity (assuming $U_i^* \simeq U_i$) shows that $V_i = U_i$ is a solution to (9) for the homogeneous shear flow. In contrast, substituting (2) in (9) indicates that $V_i = U_i$ is *not* a solution for the particle mean velocity in plane strain and axisymmetric flows. This indeed complicates the analysis for these flows and limits our discussion to small particle Reynolds numbers for which we can assume $f \simeq 1$ to a good approximation. Under this condition, by considering one-way coupling only and assuming that the initial fluctuating velocity of the dispersed phase is isotropic, Barré et al. [6] show that the particle mean velocity in plane strain axisymmetric flows can be described as $V_\alpha = \sigma_\alpha(t) x_\alpha$, where [7]

$$\sigma_\alpha(t) = \frac{(\beta_\alpha - V^0_{\alpha,\alpha})\eta_\alpha \exp(\eta_\alpha t) - (\eta_\alpha - V^0_{\alpha,\alpha})\beta_\alpha \exp(\beta_\alpha t)}{(\beta_\alpha - V^0_{\alpha,\alpha})\exp(\eta_\alpha t) - (\eta_\alpha - V^0_{\alpha,\alpha})\exp(\beta_\alpha t)}, \tag{10}$$

$$\beta_\alpha = \frac{-1 + \sqrt{1 + 4U_{\alpha,\alpha}\tau_p}}{2\tau_p}, \quad \eta_\alpha = \frac{-1 - \sqrt{1 + 4U_{\alpha,\alpha}\tau_p}}{2\tau_p}, \tag{11}$$

for $1 + 4U_{\alpha,\alpha}\tau_p > 0$,

$$\sigma_\alpha(t) = \frac{V^0_{\alpha,\alpha} - \left(V^0_{\alpha,\alpha} + \frac{1}{2\tau_p}\right)\frac{t}{2\tau_p}}{1 + \left(V^0_{\alpha,\alpha} + \frac{1}{2\tau_p}\right)t}, \tag{12}$$

for $1 + 4U_{\alpha,\alpha}\tau_p = 0$, and

$$\sigma_\alpha(t) = \frac{2\omega\tau_p V^0_{\alpha,\alpha} - (V^0_{\alpha,\alpha} - 2U_{\alpha,\alpha})\tan(\omega t)}{2\omega\tau_p + (1 + 2\tau_p V^0_{\alpha,\alpha})\tan(\omega t)}, \tag{13}$$

$$\omega = \frac{\sqrt{|1 + 4U_{\alpha,\alpha}\tau_p|}}{2\tau_p} \tag{14}$$

for $1 + 4U_{\alpha,\alpha}\tau_p < 0$. Here $V^0_{\alpha,\alpha}$ is the initial value of $\sigma_\alpha(t)$, and in our simulations, we have used

$$V^0_{\alpha,\alpha} = \begin{cases} \dfrac{1}{2\tau_p}\left(-1 + \sqrt{1 + 4U_{\alpha,\alpha}\tau_p}\right), & \text{when } U_{\alpha,\alpha} \geqslant 0, \\ U_{\alpha,\alpha}, & \text{otherwise.} \end{cases} \tag{15}$$

The above discussion assumes the homogeneity of the flow, valid only under certain conditions which can be determined by considering the transport equation for the carrier-phase fluctuating velocity

$$\frac{\partial u_i}{\partial t} + U_{i,j}u_j + U_{j,m}x_m\frac{\partial u_i}{\partial x_j} = -\frac{\partial p}{\partial x_i} + \frac{1}{Re_0}\frac{\partial^2 u_i}{\partial x_j \partial x_j} - \frac{\partial(u_i u_j - \langle u_i u_j \rangle)}{\partial x_j}, \tag{16}$$

where we have substituted $U_i = U_{i,j}x_j$, $U_{i,j} = \partial U_i/\partial x_j$. For simplicity, here we have dropped the two-way coupling term, however, it can be shown that for homogeneous shear flow the following discussion is also applicable with the inclusion of this term (see also [9]). The dependency on the coordinates x_i is explicit in (16). To remove this dependency, we apply the coordinate transformation

$$\xi_i = B_{ij}(t)x_j, \tag{17}$$

Table 1
Parameter values considered in simulations of set I for homogeneous shear flow with monosize particles

Case	Φ_m	τ_p	$N_p \times 10^{-5}$
SM1	0	0.5	1.0
SM2	0.25	0.5	3.33
SM3	0.5	0.5	6.67
SM4	0.25	1.0	1.19

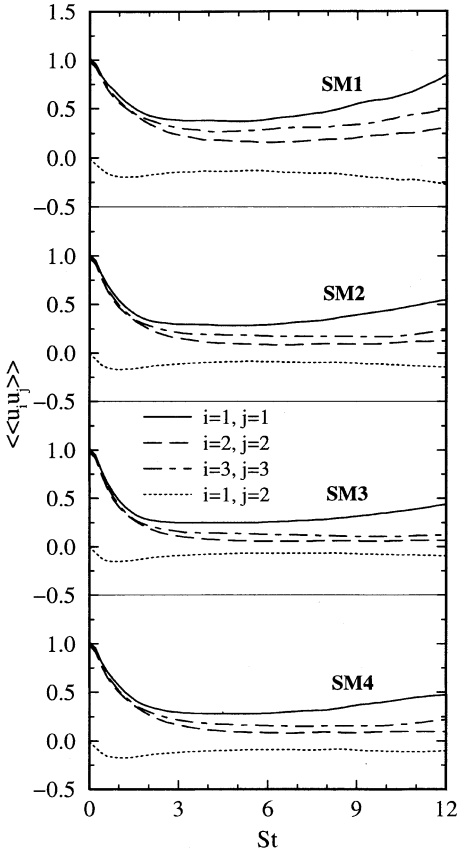

Fig. 1. Temporal evolution of fluid Reynolds stresses for homogeneous shear flow with monosize particles.

to obtain

$$\frac{\partial u_i}{\partial t} + \left(\frac{\mathrm{d}B_{mn}(t)}{\mathrm{d}t} + B_{mj}(t)U_{j,n}\right)\frac{\partial u_i}{\partial \xi_m}x_n = -B_{mi}\frac{\partial p}{\partial \xi_m} + \frac{1}{Re_0}B_{mj}B_{nj}\frac{\partial^2 u_i}{\partial \xi_m \partial \xi_n} - B_{mj}\frac{\partial(u_i u_j - \langle u_i u_j\rangle)}{\partial \xi_m} - U_{i,j}u_j. \tag{18}$$

Now, for constant mean velocity gradients, the dependency on x_i can be eliminated by requiring that

$$\frac{\mathrm{d}B_{mn}(t)}{\mathrm{d}t} + B_{mj}(t)U_{j,n} = 0. \tag{19}$$

Then, with the mean velocity given by (1) and (2), we find that

$$B_{ij}(t) = \begin{pmatrix} 1 & -U_{1,2}t & 0 \\ 0 & 1 & 0 \\ 0 & 0 & 1 \end{pmatrix}, \tag{20}$$

for the homogeneous shear flow, and

$$B_{ij}(t) = \begin{pmatrix} B^0_{11}\exp(-U_{1,1}t) & 0 & 0 \\ 0 & B^0_{22}\exp(U_{2,2}t) & 0 \\ 0 & 0 & B^0_{33}\exp(-U_{3,3}t) \end{pmatrix}. \tag{21}$$

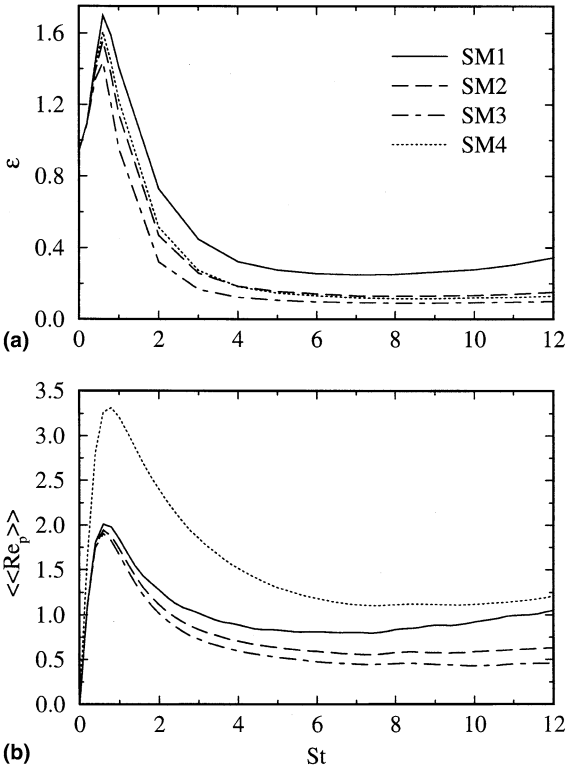

Fig. 2. Temporal evolution of (a) viscous dissipation rate and (b) particle Reynolds number for homogeneous shear flow with monosize particles.

for the plane strain and axisymmetric flows with their respective $U_{\alpha,\alpha}$ values. Here the superscript 0 indicates the initial value, i.e. $B_{ij}^0 = B_{ij}(0)$. Thus, the calculation of the fluid fluctuating velocity in the moving coordinate ξ_i does not depend on the coordinates and any statistics of u_i remains unchanged with respect to ξ_i. As a result, the carrier phase is homogeneous in the moving coordinate.

Applying the transformation to the particle momentum equation we obtain

$$\frac{dv_i}{dt} = \frac{f}{\tau_p}(u_i^* - v_i) - V_{i,j}v_j, \tag{22}$$

where for the axisymmetric flows $f = 1$ is used. For a (spatially) constant particle mean velocity gradient, the right-hand side of this equation does not show any dependency on position. Therefore, if the initial particle fluctuating velocity is homogeneous, the evolution of v_i is independent of ξ_i and the turbulence remains homogeneous. In the shear flow, the particle mean velocity is also constant in time and the same as that of the fluid, thus the moving coordinate (and the homogenous domain associated with that) evolves with the same rate for both phases. For the plane strain and axisymmetric flows, however, the particle phase evolves with a different rate than that of the carrier phase. In fact, Barré et al. [6] show that the size of the particle domain decreases in time due to the "compressibility" effect demonstrated by the mean velocity of the dispersed phase.

For the homogeneous shear flow, we simply solve (22) in the moving coordinate system. For the homogeneous

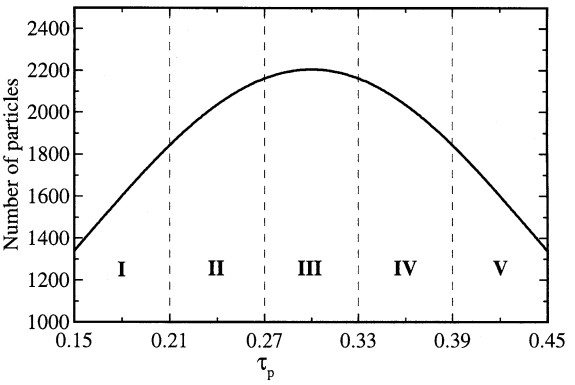

Fig. 4. Particle size distribution for polydispersed homogeneous shear case.

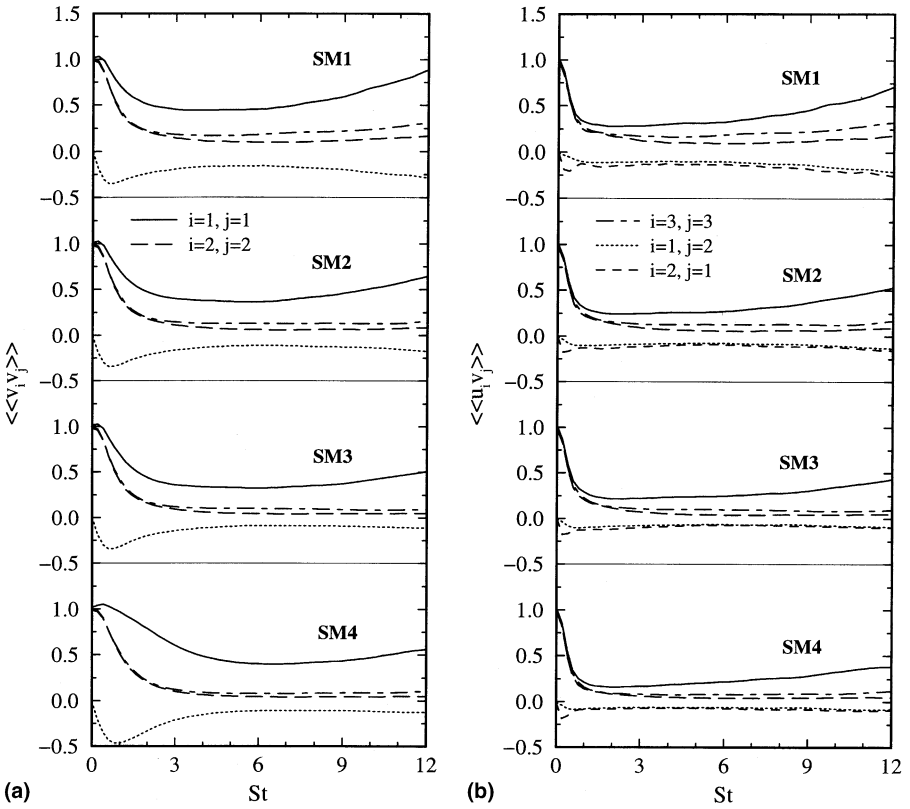

Fig. 3. Temporal evolution of (a) particle Reynolds stresses and (b) cross-correlation of velocity fluctuations of the two phases for homogeneous shear flow with monosize particles.

plane strain and axisymmetric flows, the fluid fluctuating velocity u_i is calculated in the coordinate system $O-\xi_1\xi_2\xi_3$ and, with a priori knowledge of the mean velocity U_i, the instantaneous fluid velocity can be calculated using $\widehat{U}_i = U_i + u_i$. The instantaneous particle velocity $\widehat{V}_i$ is directly obtained from solving Lagrangian particle equation (8) in the inertial coordinate system $O-x_1x_2x_3$ and the corresponding fluctuating particle velocity v_i is calculated by $v_i = \widehat{V}_i - V_i$. The computational domain in the $O-\xi_1\xi_2\xi_3$ coordinate system is $\vec{\xi} \in [0,2\pi]\times[0,2\pi]\times[0,2\pi]$. To ensure that fast Fourier transform (FFT) routines can be applied, this computational domain is fixed during the simulation.

3. Simulations and statistics

Five sets of simulations are considered: one for each plane strain or axisymmetric flows and two for shear flow. All the simulations are performed using a Fourier pseudospectral method and periodic boundary conditions are implemented for both phases. The Lagrangian equations for the particles are integrated in time using a second-order accurate Adams–Bashforth method. To evaluate the carrier-phase variables at the particle location a fourth-order accurate Lagrange polynomial interpolation scheme is used.

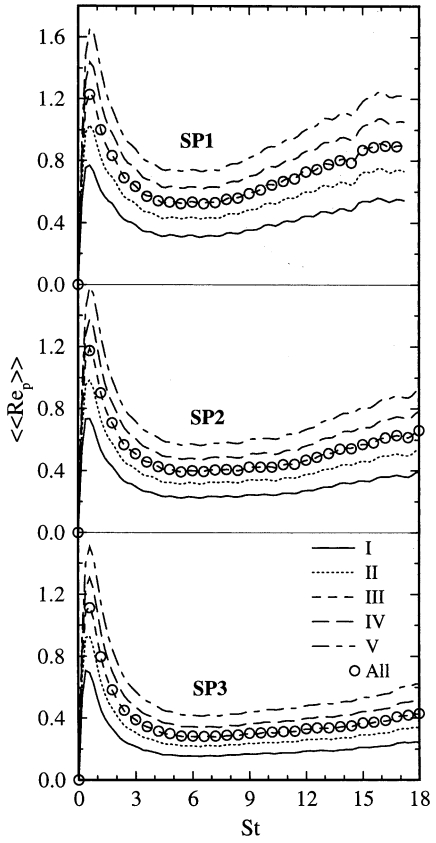

Fig. 5. Temporal variation of particle Reynolds number for homogeneous shear flow with polydispersed particles.

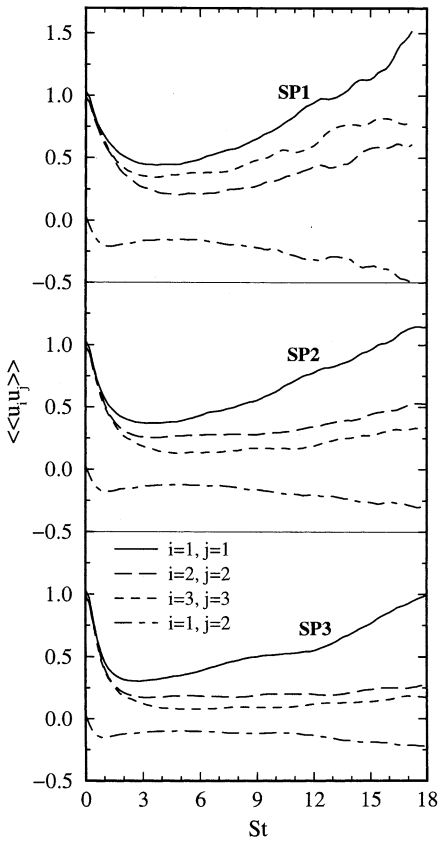

Fig. 6. Temporal evolution of fluid Reynolds stresses for homogeneous shear flow, based on all particle sizes.

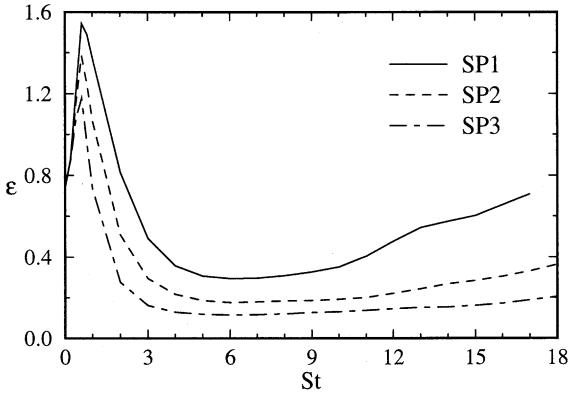

Fig. 7. Temporal evolution of viscous dissipation rate for homogeneous shear flow, based on all particle sizes.

3.1. Homogeneous shear flow

The simulations of homogeneous shear flow are directly started from a random isotropic velocity field for the carrier phase, seeded with particles which are distributed randomly with the same velocity as that of their surrounding fluid elements. The mean velocity gradient is $S = U_{1,2} = V_{1,2} = 2$, and both phases are simulated on a moving grid which continuously deforms with the mean velocity. In order to allow the simulations to progress for a substantial time, it is necessary to remesh the grid at regular time intervals [10]. The simulations are continued until the length scales of turbulence become too large to be accurately resolved. The magnitude of the mean shear and all of the initial gas-phase conditions are held constant in all the simulations.

Two different sets of simulations are considered for the homogeneous shear flow. The first set includes simulations of monosize particles at various values for the particle time constant and mass loading ratio (Φ_m, defined as the ratio of the mass of the particles and the mass of the fluid). All the simulations of this set are performed using 96^3 collocation points, with $\rho_p = 721.8$ and $Re_0 = 200$. A listing of the simulation parameters along with the total number of particles (N_p) used for each case, is given in Table 1. Here, $\Phi_m = 0$ refers to a case with one-way coupling. The simulations of Table 1 can be used to investigate the effects of the mass loading ratio and the particle time constant. The statistics generated from these simulations, are presented in Figs. 1. Since a modified drag coefficient is used for the simulations of homogeneous shear flow, in Fig. 2b we provide the temporal variation of the mean particle Reynolds number $\ll Re_p \gg$ to be used for the calculation of the coefficient f in Eq. (8).

The temporal variation of various Reynolds stresses in the homogeneous shear flow can be explained by considering their transport equations. For the carrier phase, these equations can be stated as [1]

$$\frac{\partial}{\partial t} \ll u_1^2 \gg = -2 \ll u_1 u_2 \gg U_{1,2} - \frac{2}{3}\epsilon - \frac{2\Phi_m}{\tau_p}(\ll u_1^2 \gg - \ll u_1 v_1 \gg) + \Pi_{11}, \quad (23)$$

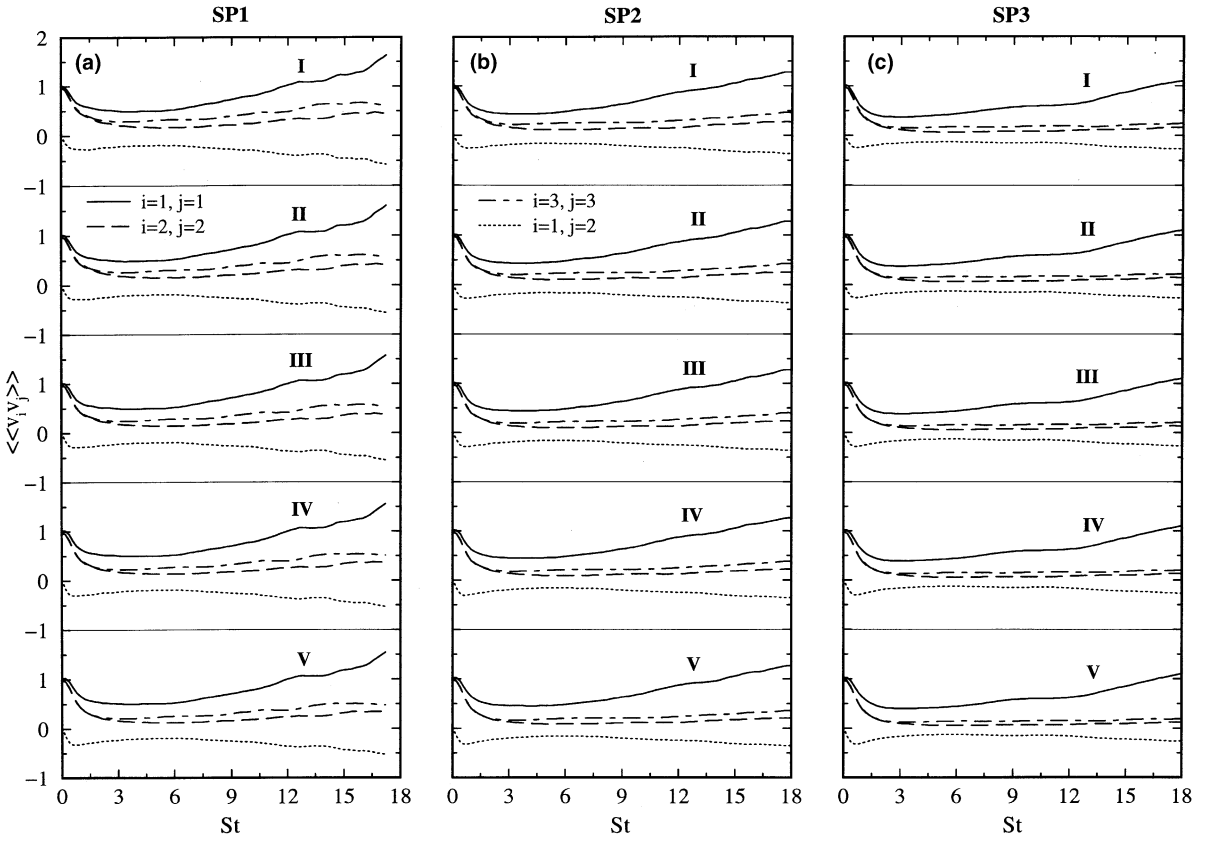

Fig. 8. Temporal evolution of particle Reynolds stresses for homogeneous shear flow with polydispersed particles for cases (a) SP1, (b) SP2, and (c) SP3.

$$\frac{\partial}{\partial t}\ll u_2^2\gg = -\frac{2}{3}\epsilon - \frac{2\Phi_m}{\tau_p}(\ll u_2^2\gg - \ll u_2v_2\gg) + \Pi_{22}, \tag{24}$$

$$\frac{\partial}{\partial t}\ll u_3^2\gg = -\frac{2}{3}\epsilon - \frac{2\Phi_m}{\tau_p}(\ll u_3^2\gg - \ll u_3v_3\gg) + \Pi_{33}, \tag{25}$$

$$\frac{\partial}{\partial t}\ll u_1u_2\gg = -\ll u_2^2\gg U_{1,2} - \frac{\Phi_m}{\tau_p}(2\ll u_1u_2\gg - \ll u_1v_2\gg - \ll u_2v_1\gg) + \Pi_{12}, \tag{26}$$

where

$$\Pi_{ij} = \psi_{ij} - \left(\epsilon_{ij} - \frac{2}{3}\epsilon\delta_{ij}\right), \quad \psi_{ij} = \left\langle p\left(\frac{\partial u_i}{\partial x_j} + \frac{\partial u_j}{\partial x_i}\right)\right\rangle,$$
$$\epsilon_{ij} = \frac{2}{Re_0}\left\langle \frac{\partial u_i}{\partial x_l}\frac{\partial u_j}{\partial x_l}\right\rangle. \tag{27}$$

Here, ϵ and ψ_{ij} are, respectively, the isotropic rate of dissipation and the pressure strain-rate correlation. Notice that, the terms involving the derivatives of the fluid velocity can only be calculated by Eulerian averaging. Eqs. (23)–(26) can also represent the transport equations for the Reynolds stresses of the dispersed phase by replacing u_i with v_i everywhere except in the fluid-particle velocity correlations $\ll u_iv_j\gg$ which remain the same. Also, for the dispersed phase $\Phi_m \equiv 1$, $\epsilon \equiv 0$, and $\Pi_{ij} \equiv 0$.

Since the simulations are started with an isotropic velocity field, there is no initial shear component for the Reynolds stress. As a result, the production term $(-2\ll u_1u_2\gg U_{1,2})$ is initially zero and, according to (23), the streamwise component of the fluid Reynolds stress decays for $0 \leqslant St < \sim 2$. During this time interval, as (26) indicates, a shear component is produced due to the presence of the normal Reynolds stress $(\ll u_2^2\gg)$ in the cross-stream direction. This in turn, as witnessed in Fig. 1, causes the normal Reynolds stress in the streamwise direction to grow. The transfer of energy from the streamwise component, through the pressure strain-rate correlation, then results in the growth of the normal components in the cross-stream and spanwise directions as well. The rate of growth, however, depends on the mass loading ratio and is decreased due to the drag. This is also true for the particle Reynolds stresses and the

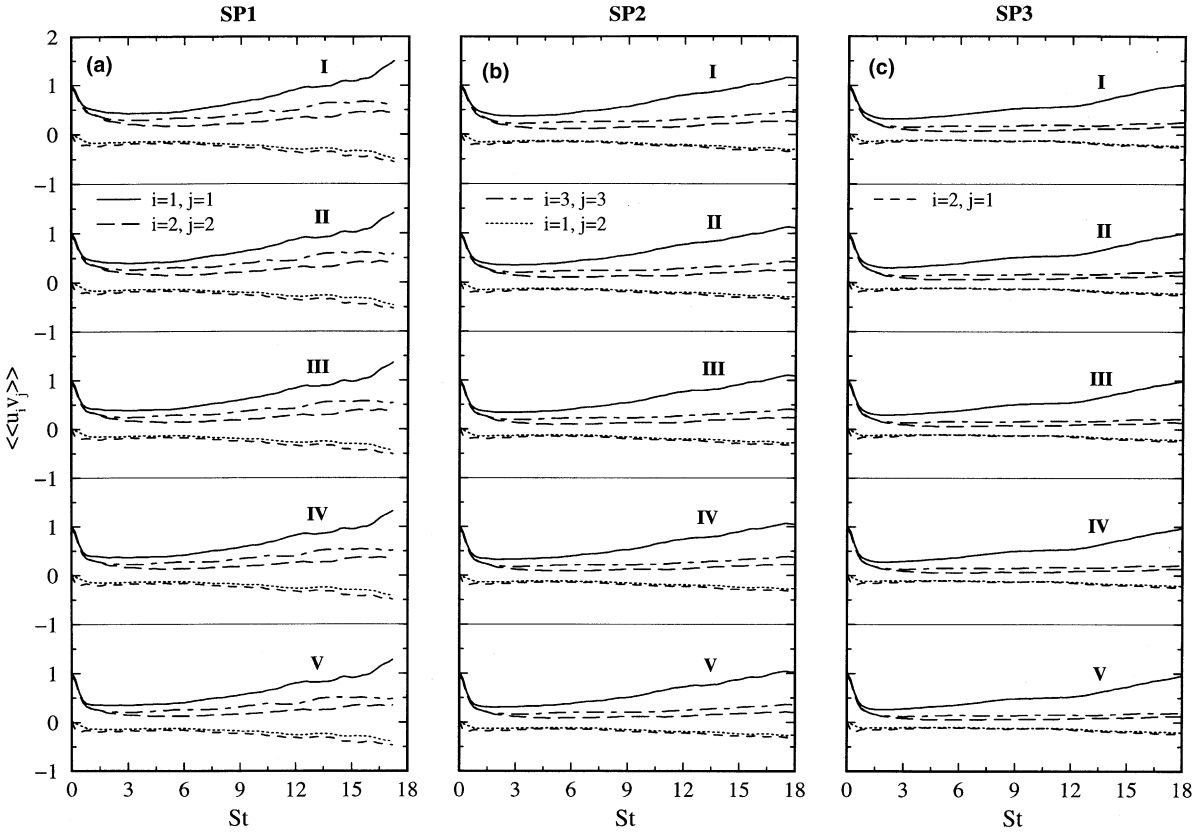

Fig. 9. Temporal evolution of cross-correlation of fluctuating velocities for homogeneous shear flow with polydispersed particles for cases (a) SP1, (b) SP2, and (c) SP3.

cross-correlation of the fluctuating velocities of the two phases (Fig. 3). The effect of the particle time constant is clearly observed by comparing the variation of $\ll v_i v_j \gg$ for cases SM2 and SM4 in Fig. 3a. It is noted that there is a peak in the variation of $\ll v_1 v_1 \gg$, the extent of which increases with the increase of the particle time constant. Although the initial Reynolds stresses of the particle phase are also isotropic, there is no viscous dissipation involved in this phase and the shear component grows much faster than that in the fluid phase, during the early stages. This increases the rate of production of the streamwise normal Reynolds stress and results in the increase of this component. After a short initial time, however, the difference in the velocities of the two phases increases and the drag term becomes more effective in decreasing the normal Reynolds stresses of the dispersed phase. Notice that there is no mechanism similar to pressure of the fluid to transfer the energy from the streamwise direction to other directions. A more modest distribution of energy is accomplished by drag.

The second set of simulations considers "polydispersed" particles with $\rho_p = 1000$ and $Re_0 = 200$. For these simulations the particle size distribution is Gaussian with a standard deviation of 0.15 and a mean value of $\ll \tau_p \gg = 0.3$. To avoid too small or too large particles, the distribution is bounded by $0.15 \leqslant \tau_p \leqslant 0.45$ as shown in Fig. 4. One case with one-way coupling ($\Phi_m = 0$, denoted as SP1) and two cases with two-way coupling at $\Phi_m = 0.2$ and 0.6 (denoted as SP2 and SP3, respectively) are considered. The simulations of set II are performed on 128^3 grid points with $N_p = 9.44 \times 10^5$ for SP1 and SP2, and $N_p = 2.83 \times 10^6$ for SP3. These simulations are primarily designed for the assessment of statistical models for polydispersed particles. When using such models, the common practice is to divide the entire range of the particle size into smaller regions, each represented by an average particle time constant (or size). Here, we provide statistics for five different regions as indicated in Fig. 4 by I–V. The statistics in each region is calculated using the particles whose time constant is located within that region. For reference, we have also considered the statistics calculated based on all the particles.

The temporal variation of the particle Reynolds number is shown in Fig. 5 for all of the cases and various particle size ranges. As expected, for each case the particle Reynolds number increases with the increase of the particle size. A close inspection of the results shown in Fig. 5, indicates that the statistics calculated based on all the particles (indicated by "All" in the figure) is virtually the same as that calculated using only the particles in the central region III. Further analysis of the results revealed that this is also the case for other statistics. In the following Figs. 8 and 9 we do not show the statistics calculated based on all of the particles as they are well represented by the particles of region III.

Figs. 6 and 7 provide the information pertaining to the carrier-phase Reynolds stresses and viscous dissipation rate, respectively. It should be emphasized that the fluid Reynolds stresses are calculated based on the velocity of the fluid at the particle location (shown by the superscript * in the previous section). An analysis of the results indicated that the fluid Reynolds stresses for various particle regions are very close, thus here we only present the statistics calculated using all of the particles. The particle Reynolds stress and the fluid-particle correlations, however, are directly affected by the size of the particles and are presented separately for various regions in Figs. 8 and 9. The general behavior of the

Table 2
Parameter values considered in the simulations of the plane strain flow

Case	τ_p	$V^0_{1,1}$	$V^0_{2,2}$	$V^0_{3,3}$	$N_p \times 10^{-5}$
PS1	0.112	0.686	−0.739	0	1.2
PS2	0.225	0.645	−0.739	0	1.2
PS3	0.372	0.603	−0.739	0	1.2
PS4	0.434	0.588	−0.739	0	1.2

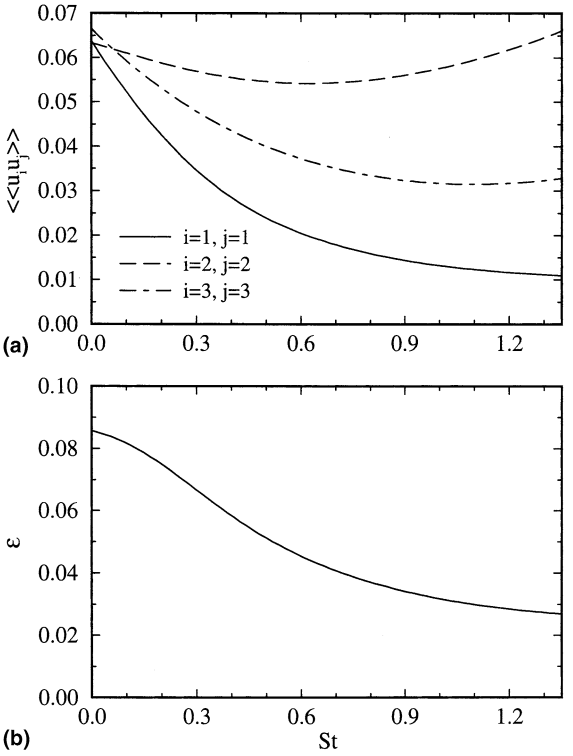

Fig. 10. Temporal evolution of (a) fluid Reynolds stresses and (b) viscous dissipation rate for homogeneous plane strain flow.

statistics in set II is analogous to that observed in set I and may be explained similarly. It should be noted that the particle time constants are smaller for set II and, by using a higher resolution, we have been able to continue the simulations of this set for a longer time.

3.2. Homogeneous plane strain flow

The initial conditions for the plane strain flow simulations are obtained by performing simulations of decaying turbulence. The initial (random) velocity field for the carrier phase, in decaying simulations, is generated in the Fourier space. The computational domain is elongated (shortened) in the direction of positive (negative) mean strain rates during plane strain flow simulations. To allow the simulations to continue for a longer time, we implement a predistorted initial mesh with the aspect ratio 1/2:2:1 ($B^0_{11} = 2,\ B^0_{22} = 1/2,\ B^0_{33} = 1$). This aspect ratio is kept the same during the decaying simulations. For the plane strain simulations this initial aspect ratio gradually evolves into 2:1/2:1 ($B_{11} = 1/2, B_{22} = 2, B_{33} = 1$) at the final time when the reference total strain $c = \exp(St)$ reaches approximately 4. The initial turbulence kinetic energy and its dissipation rate (as determined at the end of the decaying simulations) for the plane strain simulations are $k = \langle u_i u_i \rangle/2 = 0.097$ and $\epsilon = 0.0857$, respectively. To initiate the plane strain flow simulations, the carrier phase mean velocity gradient with $S = U_{1,1} = -U_{2,2} = 0.739$ is imposed and the particles are distributed randomly with the same fluctuating velocity as that of their surrounding fluid elements. The initial mean velocity gradient of the dispersed phase is imposed as

$$V_{i,j}(0) = \begin{pmatrix} \beta_1 & 0 & 0 \\ 0 & -S & 0 \\ 0 & 0 & 0 \end{pmatrix}, \tag{28}$$

where β_1, given by (11) for $\alpha = 1$, is the asymptotic mean velocity gradient for the dispersed phase in the x_1 direction and does not change in time [6]. The initial mean velocity gradient in the x_2 direction, however, is not the asymptotic value and the mean velocity gradient in this direction evolves in time according to (10) with $\alpha = 2$.

All the simulations of the plane strain flow are performed using 160^3 collocation points with the total number of particles as shown in Table 2. Also, for all of the

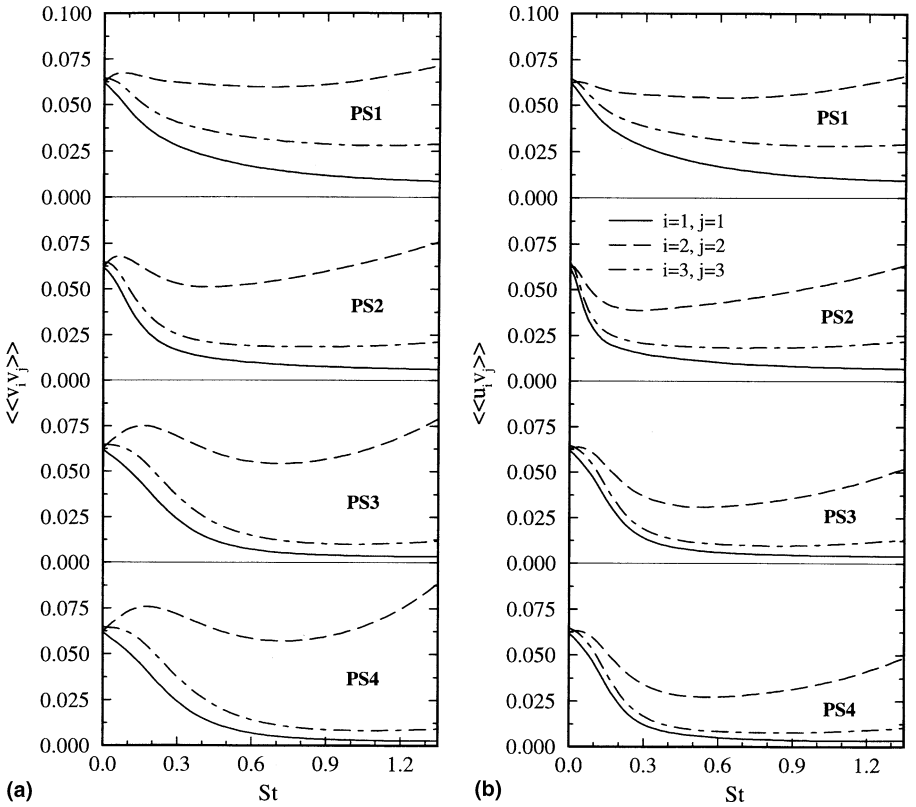

Fig. 11. Temporal evolution of (a) particle Reynolds stresses and (b) cross-correlation of velocity fluctuations of the two phases for homogeneous plane strain flow.

cases $\rho_p = 721.8$ and $Re_0 = 536.1$. The statistics generated from the simulations of the plane strain flow are presented in Figs. 10 and 11. Only the statistics of interest in the assessment of statistical/stochastic models are discussed here. These include the carrier phase Reynolds stresses $\ll u_i u_j \gg$ and the viscous dissipation rate ϵ in Fig. 10. Notice that only one-way coupling is considered and the fluid statistics remain the same for all of the cases. The information provided in Fig. 10 may be utilized for the assessment of turbulence models for the fluid phase, or it may be considered as a direct input to the models so that one can focus on the assessment of the models for the dispersed phase. In the former approach, the data at an early time are treated as the initial conditions and models are required for the prediction of $\ll u_i u_j \gg$ and ϵ in later times (see e.g. [1]). In the latter approach, the data from Fig. 10 are used as they are presented here and models are needed for the prediction of the dispersed phase Reynolds stresses $\ll v_i v_j \gg$. This process usually requires (explicitly or implicitly) the calculation of the cross-correlations of the fluid and particle fluctuating velocities $\ll u_i v_j \gg$. This information is provided in Fig. 11.

3.3. Homogeneous axisymmetric flows

We have recently conducted DNS of homogeneous, axisymmetric contraction and expansion turbulent flows laden with solid particles. The results are reported in [7] in a format applicable for model validation and will not be presented here for brevity. The numerical procedure is very similar to that adopted in [6], however, only the carrier phase is simulated during the decaying simulations of axisymmetric flows. The particles are introduced into the flow field obtained at the end of the decaying simulations, and are randomly distributed with a zero velocity relative to the local fluid. All the simulations are conducted with $Re_0 = 232.6$, $\rho_p = 721.8$, and $N_p = 1.2 \times 10^5$ on 128^3 collocation grid points.

4. Conclusions

A comprehensive data bank from numerical simulation of homogeneous particle-laden turbulent flows, which can be used for the assessment of various stochastic/statistical models, is reported. Statistics from the simulations of homogeneous shear flow and homogeneous plane strain flow are presented, while for the homogeneous axisymmetric case we refer to our previous works.

For homogeneous shear flow we consider two sets of simulations for monodispersed and polydispersed particulate phase. For the first set, we present four cases having different mass loading ratios and particle time constants. The particle Reynolds stresses for the dispersed phase and cross-correlation of the fluctuating velocities of the two phases show similar behavior. The rate of production of streamwise normal stresses in the particle phase is higher than that in the fluid phase due to the larger growth rate of the shear component as a result of the absence of any viscous dissipation in the dispersed phase.

In the polydispersed set we consider three cases with different values of particle mass loading. In order to study the effect of droplet size distribution, we consider a Gaussian distribution and divide the entire range into five subranges, each represented by an average particle time constant. The analysis of the results reveal that the statistics based on all of the particles is the same as that calculated using particles in the region centered around the mean particle size. The fluid Reynolds stresses for the various particle regions are very close, whereas the particle Reynolds stresses and fluid-particle correlations exhibit strong dependence on the particle size. The qualitative behavior of the statistics presented for polydispersed set is similar to the monodispersed set.

For the plane strain flow we analyze cases with one-way coupling but with various particle time constants. The carrier phase Reynolds stresses and viscous dissipation remain the same for all the four cases considered. The above quantities may be utilized for assessing various turbulence models for the fluid phase or as input parameters for assessment of dispersed phase models. The dispersed phase Reynolds stresses and cross-correlation of the two phases, which would serve as the benchmark for the accuracy of the dispersed phase models, are also presented.

Acknowledgements

This work was supported through grants N00014-05-1-0253 and CTS-0237951 from the Office of Naval Research and the National Science Foundation, respectively. The computational resources were provided by the San Diego Supercomputing Center.

References

[1] F. Mashayek, D.B. Taulbee, Turbulent gas–solid flows. Part II: Explicit algebraic closures, Numer. Heat Transfer, Part B 41 (1) (2002) 31–52.
[2] R.V.R. Pandya, F. Mashayek, Non-isothermal dispersed phase of particles in turbulent flow, J. Fluid Mech. 475 (2003) 205–245.
[3] Z. Gao, F. Mashayek, Stochastic model for non-isothermal droplet-laden turbulent flows, AIAA J. 42 (2) (2004) 255–260.
[4] M.J. Lee, W.C. Reynolds, Numerical experiments on the structure of homogeneous turbulence, Department of Mechanical Engineering Report TF-24, Stanford University, Stanford, CA, 1985.

[5] C. Barré, Direct numerical simulation of particle-laden plane strain turbulent flows, M.S. Thesis, Department of Mechanical and Aerospace Engineering, State University of New York at Buffalo, Buffalo, NY, 1998.
[6] C. Barré, F. Mashayek, D.B. Taulbee, Statistics in particle-laden plane strain turbulence by direct numerical simulation, Int. J. Multiphase Flow 27 (2) (2001) 347–378.
[7] S. Liao, F. Mashayek, D. Guo, Numerical simulations of particle-laden axisymmetric turbulent flows, Numer. Heat Transfer, Part A 39 (8) (2001) 847–855.
[8] R. Jackson, Locally averaged equations of motion for a mixture of identical spherical particles and a Newtonian fluid, Chem. Eng. Sci. 52 (15) (1997) 2457–2469.
[9] F. Mashayek, Droplet-turbulence interactions in low-Mach-number homogeneous shear two-phase flows, J. Fluid Mech. 367 (1998) 163–203.
[10] R.S. Rogallo, Numerical experiments in homogeneous turbulence, NASA TM 81315, 1981.